

A 60 GHz pulsed coherent radar for online monitoring of the withering condition of leaves



N.A. Hoog^{a,*}, T.E. van den Berg^{b,1}, H.S. Bindra^a

^a Integrated Circuit Design (ICD), Faculty of Electrical Engineering, Mathematics and Computer Science (EEMCS), University of Twente, Enschede, the Netherlands

^b Integrated Devices and Systems (IDS), Faculty of Electrical Engineering, Mathematics and Computer Science (EEMCS), University of Twente, Enschede, the Netherlands

ARTICLE INFO

Keywords:
Pulsed coherent radar
Plant leaf withering
Water content

ABSTRACT

This paper introduces a novel sensor application for online monitoring of the withering condition of leaves. The proposed system is based on the millimeter-wave radar sensitivity and its signal variations that correlate with the water content in a leaf. To validate the experimental prototype, a 60 GHz pulsed coherent radar (PCR) coupled with a dielectric lens was configured. The data obtained by means of the radar sensor is correlated with the data of the conventional gravimetric using a modelling approach based on Beer-Lambert's law. To the best of our knowledge this is the first proof-of-concept demonstrating the relation between the received signal amplitude from the millimeter-wave radar sensor and plant leaf mass loss.

1. Introduction

Despite many studies [1,2] carried in the field of monitoring plant leaf water content and its withering, a large gap remains between commercially-available monitoring techniques and state-of-the-art research.

In particular, there are only a few sensors that are designed specifically for monitoring the withering conditions of a leaf. Table 1 itemizes some of the commonly used systems currently available [3–8].

In recent years, there has been an increasing interest in highly integrated radar sensors operating in millimeter-wave frequency band [9–12]. By virtue of their small size, low-power consumption, and relatively simple implementation, such millimeter wave radars reveal possibilities that may be employed in the next generation of sensors for food, agriculture, and horticulture sectors [13–19].

Here we explore the water content changes of withering leaves as a novel application for highly integrated and commercially available pulsed coherent radar (PCR) at 60 GHz. It can be of great interest e.g. for tea manufacturers, drying herbs where it can be embedded in the conveyor belt type (microwave) oven, or it even might be considered as a part of non-invasive plant health condition assessment systems. Basic characteristics of the suggested sensor application using 60 GHz pulsed coherent radar (PCR) are given next to the available sensor platforms in the Table 1.

In general, radar systems are known for being able to perform under different weather and storage conditions. Also, they can be used in the day or night time providing accurate and precise measurements [20]. These characteristics are important and beneficial for the proposed applications [21,22].

The advantage of using a pulse radar over continuous – wave(CW) radar is that pulse radar operates in the time domain and therefore it does not require the fast Fourier transform (FFT) analysis that characterizes CW radar [23]. Without excessive computational needs a highly-integrated radar system can be implemented using low-power microcontrollers [24].

The spectrum available in the 60 GHz band is license-free, the most open and favourable for industrial design applications compared to other frequency bands used for radar sensors, e. g. at 24 or 77 GHz [25–27].

Moreover, 60 GHz millimeter-wave systems are promising for indoor communication where increasing data transmission speed is needed and can be used for short-range applications for example for the internet of things (IoT) and other platforms for automatic remote data collection [28].

When a specific radar application is proposed, it is also important to consider effects such as the gaseous attenuation for oxygen absorption and for water vapor absorption as a function of range. In particular, the resonances for frequencies below 100 GHz occur at near 22 GHz for

* Corresponding author.

E-mail address: n.hoog@utwente.nl (N.A. Hoog).

¹ ORCID: 0000-0002-7202-4699.

water vapor (H_2O) and 63 GHz for oxygen (O_2) [29]. Attenuation due to water vapor is a strong function of temperature, pressure, and humidity. Since this work focuses on measuring changes of a water content in the leaf and not the properties of surrounding vapor or gas in its environment, the choice for 60 GHz over 24 can be decisive.

In comparison to other candidates [30,31] the Acconeer 60 GHz pulsed coherent radar (PCR) is a low power System-in-Package (SiP) with the integrated baseband, radio frequency (RF) front-end, and antenna in package (AiP) [32]. It makes for a cost-effective and compact solution for sensing.

Although, integrated PCR is not so widespread as solutions based on frequency-modulated continuous-wave (FMCW) radar operating at 24 GHz [33–35], 60 GHz [36], 77 GHz [37,38] numerous fascinating and practical applications have been reported [24,39–42] and further interest is growing in different industry sectors different industry sectors including agriculture and horticulture [43,44].

Regarding the assessment process for leaf withering monitoring itself, primarily, the relative water content (RWC) is the most examined parameter [45]. The RWC is defined in [45,46] as a ratio of the amount of water in the leaf tissue at sampling to that present when fully turgid. Conventionally, the RWC is measured with gravimetric techniques using different load cells [47]. These measurements rely on an intensive sampling of an individual leaf and a time - consuming exchange between the collected data and their analysis. This is a main limitation of the RWC method [45]. Microwave sensing offers a good alternative to these measurements as it may provide information over a large number of leaves, timely and cost-effective means for leaf withering monitoring. In particular, the microwave radar technologies are suitable for monitoring of the withering condition of leaves through the signals that are operating between the frequency range of 30 and 300 GHz that offer high sensitivity due to the absorptions. Thus, the radar sensor signature depends to a large extent on the physical and chemical characteristics of its surrounding matter. Accordingly, the property of water to absorb microwave energy ensures that the radar signal response exhibits sensitivity towards the water content. Therefore, a major part of this research is to relate the measured mass loss in the conventional gravimetric techniques to estimate the relative water content (RWC) and the decrease of the amplitude signal obtained by the radar sensor, namely 60 GHz PCR, using Beer-Lambert's law [48,49].

The suggested relation explains the new modelling approach and facilitate the use of millimeter waves sensors for the plant leaf withering monitoring. While there is a prior research on assessing plant water content using a highly - integrated radar presented in [50], it is limited to experimental tests and no physico - mathematical models were implemented.

Furthermore, unlike the gravimetric methods the proposed radar

sensor application is based on the evaluation of the RWC in plant leaves without weighing of an individual leaf. Assuming that the monitored leaves are of the same species, then the key advantage of this sensor based on millimeter - wave radar is the ability to accomplish results with the least amount of wasted time, effort, and competency in performance. After performing initial measurements on one saturated leaf and one dry leaf, it is possible to use this as a basis to convert all current water content measurements into relative water content measurements [45]. RWC is often used as a reference method [51] and was applied in this study to prove the feasibility and applicability of the proposed system.

In this way, a 60 GHz pulsed coherent radar (PCR) and the new modelling approach, provides valuable insights into a development of online, compact, simple to use and maintain, reliable, low-cost sensing platform for the plant leaf withering monitoring.

2. Materials and methods

2.1. 60 GHz PCR sensor experimental prototype setup

Fig. 1 shows the layout of the experimental prototype setup. This setup consists of the following parts: 60 GHz pulsed coherent radar (PCR), built-in XM112-XB112 module evaluation kit (EVK) based on the highly – integrated radar A111 [34], supplied with two dielectric lenses and one flat cover of the LH112 radar lens kit (Fig. 2), designed and manufactured by Acconeer, detailed description of properties and expected performances can be found in [52,53].

The lens performances are conditional to the distance from the

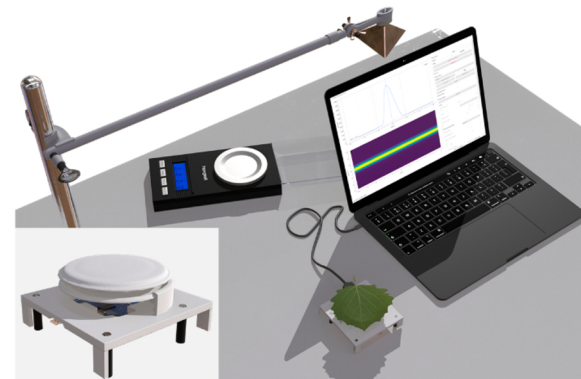


Fig. 1. Prototype configuration used in experiments. The inset shows the zoomed view of the evaluation kit assembled with the dielectric lens without applying a plant leaf on top.

Table 1

List of commercially – available sensors to estimate water in leaves and comparison of their characteristics to the suggested sensor application.

Manufacturer	Suggested sensor application	Stesalit Systems Limited	Agrihouse Brands ltd	METER Environment
Model	–	TWMAC ^a [3]	^b AH-300w2 [4] ^c AH-300 [5] ^d AH-303 [6]	^e Phytos 31 (LWS-17-PT) [7,8]
Technique	60 GHz PCR	weight and temperature sensors	hall - effect sensor	capacitive sensor
Individual leaf measurements	yes	no	yes (only for wetness of leaf surface)	yes (only for an small amount of surface water – wetness of leaf)
Bulk volume or a set of multiple leaves measurements	yes (shown only for a set of multiple leaves)	yes	no	yes (only for an small amount of surface water – wetness of leaf surface)
Online monitoring	yes	yes	yes	yes
Size	miniaturized	bulky	miniaturized	compact

^a Tea Withering Monitoring and Control System.

^b Leaf Sensor and Wireless Device Cloud Package.

^c Leaf Sensor Rev3 w/connector, cable and software CD-ROM.

^d Leaf Sensor Rev3 - bare wire version.

^e LWS Meter Phytos 31 Leaf Wetness Sensor.

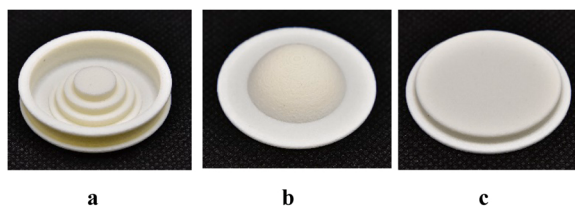


Fig. 2. The radar lens kit LH112 comprises of the following items: a) FZP lens (Fresnel Zone Plate); b) HBL lens (Hyperbolic Lens), c) flat cover. The plastic lens holder is not shown here, but can be seen in Fig. 1 as the lens mounted.

integrated antenna. In this work the construction that allows the maximum gain 9.1 [dB] and 10.0 [dB] for Fresnel Zone Plate lens (FZP lens) and Hyperbolic Lens (HBL lens), respectively, was chosen. The outlined maximum gains are relative to the free-space scenario.

The integrated antennas of A111 chip are a folded dipole type, and their functionalities are related to its ground reference in the package ground plane, extending over the whole area of the sensor [54]. It means that material or medium surrounding the sensor should have properties of a dielectric (insulator), for example, plastic or glass. It is possible to place a leaf directly on top of the A111 chip and conduct some measurements under the laboratory conditions (it will be shown later in the Section 3), but there is a high risk not only to obtain wrong results, but also to destroy the sensor applying conductive substances like a water content of a leaf.

Therefore, a radome: a structural enclosure that protects a radar assembly is needed for the final application. A dielectric lens can be an integrated part of such a radome. As a minimum requirement, the flat cover (as one included in the EVK) with the gain of -0.15 [dB] is recommended to use for the proposed application. However, the FZP lens is the beneficial candidate for such the radome of the PCR sensor because of its flatness in comparison to the HBL lens and more options for assembly in comparison to the flat cover.

Most of the work shown in this paper was performed using the FZP lens.

Depending on use case and based on different algorithms, four modes of operation are available for Acconeer pulse coherent radar: sparse, power bins, IQ, and envelope [52]. The sparse service is ideal for motion-sensing applications requiring high robustness and low power consumption. The Power Bins Service is mainly intended for use in low power applications where large objects are measured at short distances from the radar sensor. The IQ service provides capability of detecting fine movement occurring in a target scene. This service is similar to the envelope service. Though, the envelope service is optimized for providing an accurate envelope estimate, while the IQ service is optimized for producing a phase-stable estimate. Inasmuch as there is no use of phase information in the data process for monitoring of the withering condition of leaves, the envelope service was selected. The detailed description of all settings for the envelope and other services can be found in [55].

The assembled EVK was connected to a computer. A standard corner reflector with RCS of 1 m² at 60 GHz was used to fix the path-length of the radar signal from the transmit antenna of the PCR along the direction of propagation, and to make the power of the reflected signal independent to the environmental background and the other objects. A weighing scale Homgeek Professional Digital Mini Scale TL-series [56] was used to

measure the mass of studied leaves.

Table 2 lists the applied settings of the PCR sensor.

To receive and record data scripts in Acconeer Python Exploration Kit and graphical user interface (GUI) were used [57,58].

2.2. Working principle of the prototype

The working principle of the suggested PCR prototype is to detect changes in the received signal and based on the following concepts:

- 1) PCR sensor is a time-of-flight system, which means that an electromagnetic (EM) wave emitted by a transmit antenna and travels toward a target through the medium with the complex refractive index n [-]. Also, a fraction of the signal is scattered back to the sensor and recorded by a receiver antenna [23].
- 2) In general, the transmitted signal $s_t(t)$ of PCR consisting of one wavelet pulse can be expressed as follows (1):

$$s_t(t) = a_t u(t) \bullet e^{j2\pi f_0 t} \quad (1)$$

where a_t describes the amplitude factor, f_0 [Hz] is the radar carrier frequency, and $u(t)$ is the complex transmitted modulation [23].

- 3) Determined by factors such as the type of the target and distance to it r [m], the received signal $r_t(t)$ differs from the transmitted signal (1) having a different amplitude a_r , and being delayed by τ_r [s]: (2), [23]:

$$r_t(t) = a_r u(t - \tau_r) \bullet e^{j2\pi f_0 \bullet (t - \tau_r)} \quad (2)$$

- 4) In addition, the distance r [m] to the target is can be determined by time delay τ_r [s], between the transmitted and received signal (3) [23]:

$$r = c \bullet \tau_r / (2 \bullet n) \quad (3)$$

where c [m/s] velocity of light in vacuum.

The factor of-two in (3) accounts for the round trip propagation path of the pulse.

- 5) EM waves propagate through free space or a medium with an amplitude and phase corresponding to a propagation constant (γ) [m^{-1}] (4–5), [23]:

$$a_r = a_t \bullet e^{-\gamma l} \quad (4)$$

and

$$\gamma = \alpha + j\beta \quad (5)$$

where α , attenuation of propagation constant γ [Np/m]; β phase of the propagation constant γ [rad/m]; l is the distance from source [m] (in the case demonstrated in this paper and shown in Fig. 1 $l = r$, denotes the one-way path of energy from the radar to the corner reflector, but in general terms is either the direct or reflected signal).

- 6) digital values of the received signal amplitude produced as an output of the analog-to-digital converter (ADC) were recorded and analysed.

2.3. Gravimetric determination of relative water content (RWC) in a plant leaf

Estimation of relative water content (RWC) in leaves can be used to assess their withering stage [59]. The conventional gravimetric method for RWC determination in a leaf which further denoted as RWC_m , involves finding its fresh mass (FW_m), turgid mass (TW_m) and the dry mass (DW_m) as described in the Section 2.5, below. Thereafter, RWC_m can be calculated by the following (6), [60,61]:

$$RWC_m(\%) = 100 \bullet (FW_m - DW_m) / (TW_m - DW_m) \quad (6)$$

Table 2
PCR sensor settings.

Setting	Value	Unit
Range interval	0.20–0.60	[m]
Running average factor	0.70	[-]
Update rate	10	[Hz]
Background buffer length	50	[-]

2.4. Determination of RWC in a plant leaf applying the Beer-Lambert's law

The modelling approach for the assessment of the RWC using the received signal amplitude from a 60 GHz PCR sensor was derived by analogy with the conventional form of the equation to estimate the RWC (5), and further denoted as RWC_{sa} .

Taking into account that the normalized amplitude (envelope service of PCR) is used to determine RWC, its attenuation is determined by many factors, but predominantly by the attenuation constant α [Np/m] and can be defined following the Beer-Lambert law and considering a term a_b due to the reflections on the background (7):

$$a_r = a_b + a_t \bullet e^{-\alpha \bullet 2T} \quad (7)$$

When (7) is applied to materials or a medium composed by different phases (solid, liquid and gas) such as a leaf, α can be replaced by the mass attenuation coefficient $\mu = \alpha/\rho$ [$m^2 \bullet kg^{-1}$] and (7) becomes (8):

$$a_r = a_b + a_t \bullet e^{-\mu \bullet \rho \bullet 2T} \quad (8)$$

ρ [$kg \bullet m^{-3}$] is the density or bulk density of the absorber material.

Passing through a medium of thickness T [m] the incident energy intensity is exponentially attenuated with increasing penetration depth. As a thickness of a leaf T is small and the variation is small, the expression (7) can be linearized and written in the form (9):

$$a_r = a_b + a_t \bullet (1 - \mu \bullet \rho \bullet 2T) \quad (9)$$

Applying Beer-Lambert law to the proposed PCR sensor with a plant leaf under test, the density (ρ) of that leaf [kg/m^3] can be calculated using the definition of the term such as, for instance, given in [62], namely, by dividing the mass (m_L) [kg] of the leaf by its volume (V_L) [m^3] and the Eq. (9) can be presented as follows (10):

$$a_r = a_b + a_t \bullet (1 - \mu \bullet m_L / V_L \bullet 2T) \quad (10)$$

Note that the term a_b is cancelled in the normalization.

To emphasize that the Beer-Lambert law makes the replacement of the mass values in (8) with the values of signal amplitude received from the radar sensor possible, it can be pointed out that the attenuation constant of a signal α is directly proportional to the mass of a leaf (m_L) [kg] (11):

$$a_r \propto \alpha \propto m_L \quad (11)$$

Combining working principles described in the Section 2.2 and the theory characterized in the Section 2.3 and the current Section 2.5, it can be concluded that fresh mass (FW_m), turgid mass (TW_m) and the dry mass (DW_m) in Eq. (6), which is basically m_L (8–12), may be interchanged with the signal amplitude and denoted as follows: FW_{sa} is the signal amplitude with a fresh leaf applied, DW_{sa} is the signal amplitude with a dry leaf applied, and TW_{sa} is the signal amplitude with a turgid leaf applied. The equations which can be used as a new modelling approach is deduced in the following forms (12–14):

$$RWC_{sa}(\%) = 100 \bullet \frac{a_r(FW_{sa}) - a_r(DW_{sa})}{a_r(TW_{sa}) - a_r(DW_{sa})} \quad (12)$$

$$RWC_{sa}(\%) = 100 \bullet \frac{\alpha(FW_{sa}) - \alpha(DW_{sa})}{\alpha(TW_{sa}) - \alpha(DW_{sa})} \quad (13)$$

$$RWC_{sa}(\%) = 100 \bullet \frac{m_L(FW_{sa}) - m_L(DW_{sa})}{m_L(TW_{sa}) - m_L(DW_{sa})} \quad (14)$$

Both values RWC_m and RWC_{sa} will be assessed and compared later in this work.

It is worth noting, that there are many ways of writing the relationship (8). In particular, the attenuation constant α [Np/m] can be expressed as the imaginary part of the refractive index, n' [-] (15), and the wavelength of the light in free space, λ_0 [m] as (16), This relationship is also known as the Beer-Lambert-Bouguer's law [62].

$$n = n' - jn'' \quad (15)$$

where n [-] is a complex refractive index, n' [-] is the real part of the n [-].

$$\alpha = 4\pi \bullet n'/\lambda_0 \quad (16)$$

The reflectivity R [-] also depends on the refractive index n [-] of the radar target, which is a leaf in this study, and for normal incidence can be expressed as: [63,64].

$$R = [(n - 1)/(n + 1)]^2 \quad (17)$$

Surface effects, scattering, thermal properties, and other variations are presumed to be second order and not considered here.

The error in amplitude as a function of time $error(a_r, t)$ [%] is defined as the percentage of difference between the experimentally obtained and theoretically computed amplitudes (10), denoted in (18) as a_{re} , a_{rt} , respectively:

$$error(a_r, t) = 100 \bullet \{ |a_{rt} - a_{re}| / |a_{rt}| \} \quad (18)$$

2.5. Plant leaves material and samples preparation

The leaf samples of four different plant species Common ivy [65], Oakleaf hydrangea [66], Panicle hydrangea [67], and English oak [68] were examined in this work. The sets of leaves were placed and processed as present in the Table 3, shown in Fig. 3 and described in the text below – here in the Section 2.5.

All examined leaves were of various sizes, shapes, and weights.

Upon that, the set 8 was prepared in order to compare results on leaf samples of different sizes of the same plant species. The set 9 contained four sick and seven healthy samples to add diversity that was not available in the sets 1–8.

To make sure that the leaves are thoroughly saturated before initial measurements, they were immersed in tap water for 24 h. After hydration, the samples were taken out of water, well dried with tissue paper and immediately weighed and measured as fully turgid leaves, obtaining values for TW_m , TW_{sa} , respectively.

The relative water content (RWC) was estimated by weighing leaves and measuring the radar signal response, and, thereafter, obtaining values for FW_m , FW_{sa} , respectively.

Two methods were applied for drying leaves:

1. Samples were dried under ambient conditions (room temperature was about 21 °C) without any additional sample preparation, and

Table 3
The selection and arrangement of leaf sets.

Set number	Scientific plant name	Number of leaves
1	Common ivy	1
2	Common ivy	3
3	Common ivy	9
4	Oakleaf hydrangea	1
5	Oakleaf hydrangea	5
6	Panicle hydrangea	1
7	Panicle hydrangea	5
8	Oakleaf hydrangea	3
9	English oak	11

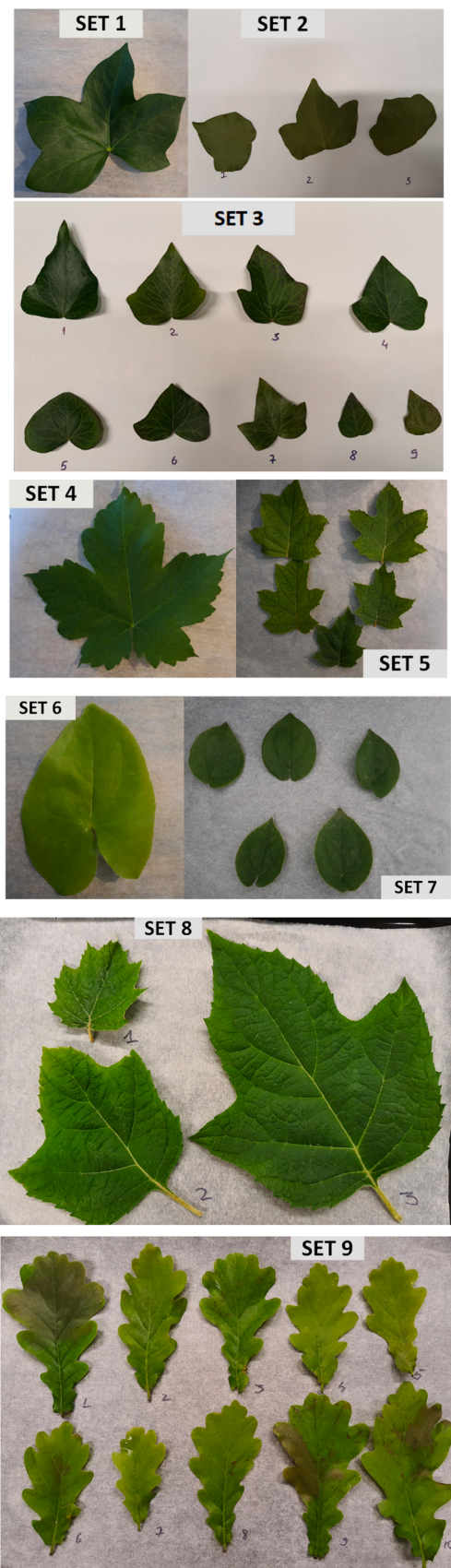


Fig. 3. Combined photo of seven sets of leaves: composed of samples from European Ivy: set 1, set 2, and set 3; Oakleaf hydrangea: set 4, set 5 and set 8; Hydrangea paniculata: set 6 and set 7, English oak: set 9.

measured every 24 h, until mass reduction of more than 90% was reached. To ensure the drying homogeneity and prevent crushing and curling of leaves during the withering process, 2 mm thick polyethylene film was placed on top of the samples. This method was performed on the sets 1–3.

2. Samples were dried in an oven at 50 °C without any additional sample preparation, and measured every 10 min, until mass reduction of more than 90% was reached. To ensure the drying homogeneity and prevent crushing and curling of leaves during the withering process, 5 mm thick metal plate of was placed on top of the samples. This method was performed on the sets 4–9.

Then the final weighing and measurements of dry leaf samples were performed, obtaining values for DW_m , DW_{sa} , respectively.

3. Results

Plots in Fig. 4 show the dynamics of an amplitude-depth response as an example of how withering of an individual leaf (set 1) can be observed on each sampling day using a 60 GHz PCR sensor prototype.

It could be seen that the amplitude of the signal increases gradually, primarily due to the decrease of the water content in the leaf sample the under test. The represented amplitude peak of the radar response at the depth of 0.4 m is determined by the position of the corner reflector according to the outline of the prototype setup shown in Fig. 1.

Similar plots could be constructed for each of the other six sets with the only difference in time frames: the interval of 10 min instead of 1 day would be used for sets 4–7.

In order to demonstrate that the suggested modelling approach is a valuable tool for estimation of the withering condition of a set of multiple samples the data were collected for two sets of Ivy leaves (set 2 and set 3): (Fig. 5. a) and one set each for Oakleaf hydrangea leaves (set 5): (Fig. 5. b) and Panicle hydrangea leaves (set 7): (Fig. 5. c) as described in the Section 2.5. All plots in Fig. 5 are based on the average values with standard error of the RWC obtained by means of the gravimetric method (RWC_m) and applying the new modelling approach (RWC_{sa}).

In addition, RWC was also estimated for the single leaf samples (set 1, set 4, and set 6) using both PCR data and mass loss measurements (RWC_{sa} and RWC_m , respectively). The results are shown in Fig. 6. for comparison purposes.

To illustrate PCR performances without a dielectric radome: either a lens or a cover, but also to compare them to the measurements applying the FZP lens, the set 8 (Oakleaf hydrangea) was prepared as described in the Section 2.5. The results of these measurements for different - sized leaves can be seen in Fig. 7.

It is obvious that the results obtained in the absence of the radome were not much different from ones acquired using the FZP lens and they

Withering of an Individual Leaf

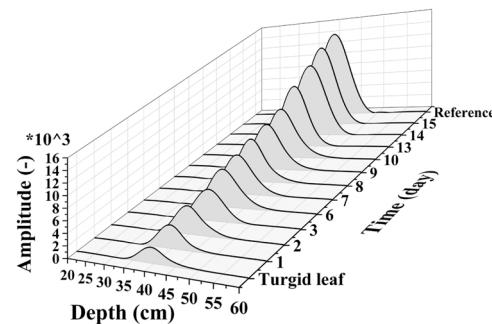


Fig. 4. A typical amplitude – depth PCR response on an individual leaf measurements per sampling date. The fully turgid leaf was drying from day 1 when it was separated from the plant. The reference measurement was performed without a leaf placed on top of the lens. The diagonal alignment of plots indicates the attenuation of the signal amplitude over the time period.

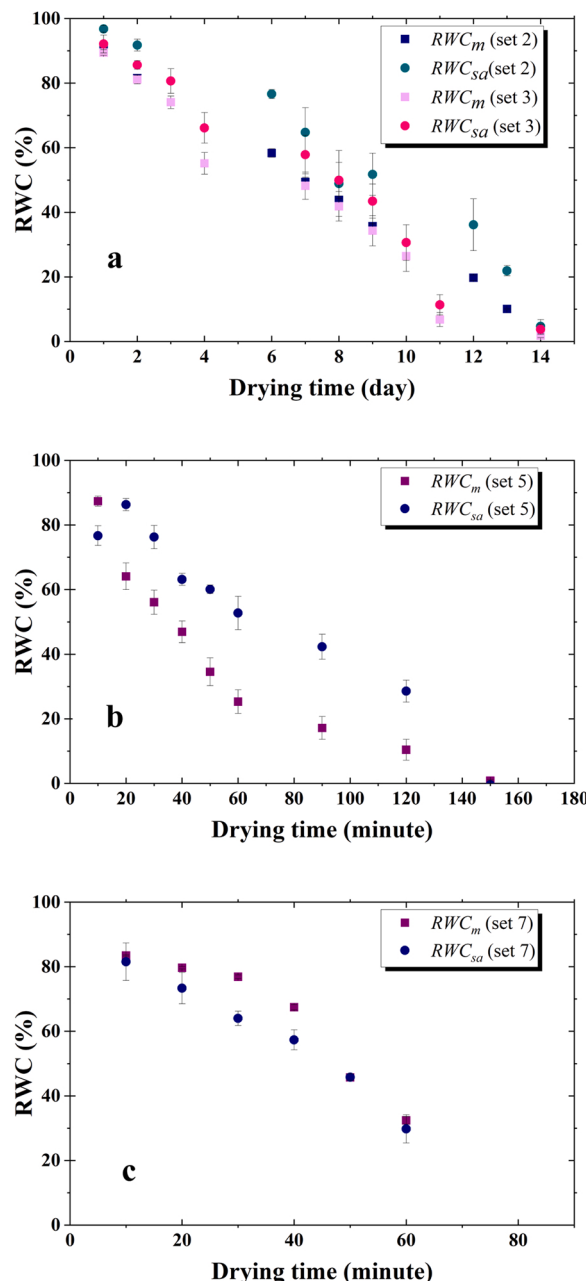


Fig. 5. Plots of water content in leaves (a: the set of Common Ivy leaves which were ambient - dried; b: the set of Oakleaf hydrangea leaves which were oven - dried; c: the set of Panicked hydrangea leaves which were oven - dried) as determined using the RWC_{sa} approach (in circles), and the gravimetric method RWC_m (in squares), as a function of drying time in a sample.

are comparable to the values of the ones obtained with the gravimetric method RWC_m : less or about 1% for the small leaf, less than 1% for the middle-sized leaf, and up to 5% for the large leaf.

In order to gain more insight to how the size of a leaf influences the obtained results, the error in amplitude between the received and expected data (18) plots were constructed as shown in Fig. 8.

The smaller error in amplitude was determined for the turgid and dry leaves which is about 2–6%. In the withering stage between 20 and 70 min the largest error in amplitude (up to 15%) was recorded at 30 min. The result was observed for all three leaves and indicate that more processes need to be considered in the model. Similar effects appeared at 50 min (up to 9%) for the large leaf and at 70 min for the small leaf (up to 4%).

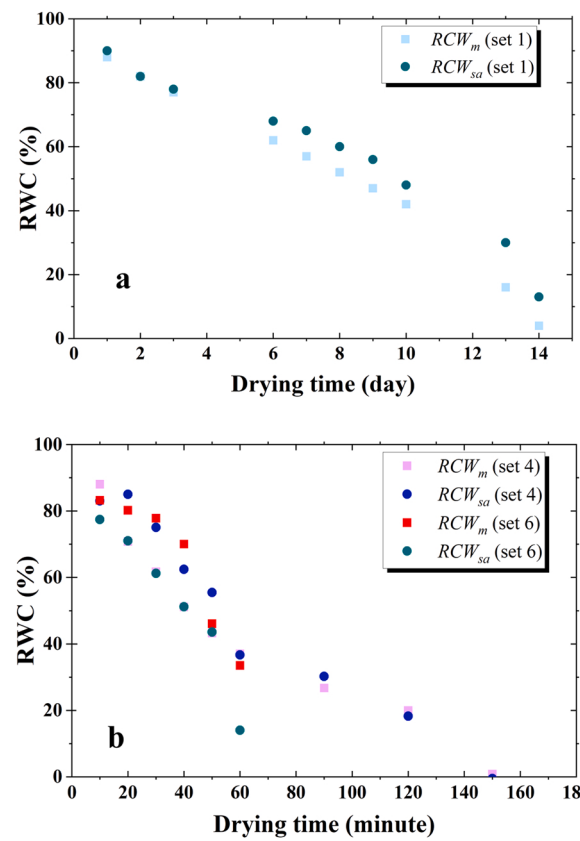


Fig. 6. Plots of water content in a single leaf as determined using the RWC_{sa} approach (in circles), and the gravimetric method RWC_m (in squares), as a function of drying time in a sample of Common Ivy (set 1, the leaf which was ambient - dried) Oakleaf hydrangea (set 4, the leaf which was oven dried); and Paniced hydrangea (set 6, the leaf which was oven - dried).

Fig. 9 presents comparison results of measurements using different types of radome as outlined in the Section 2.1 (Fig. 2). The set of English oak leaves was arranged and used as described in the Section 2.5.

Notably, the results in Fig. 9 suggest that any of the dielectric radomes: the HBL lens, FZP lens, or flat cover can be used for the proposed application, and the average values with standard error of the RWC (less than 10%) are not different from ones found for the sets 2, 3, 5, and 7. This is in agreement with measurements conducted based the set 8).

Although, the absence of a radome did not show any extreme deviations in measurements and their analysis (the R-Squared value was between 0.93%–95% in all investigated cases), it is not recommended such a setup for the for monitoring the withering condition of leaves because of reasons described in the Section 2.1.

In addition, the impact of presence of sick leaves (4 pieces out of 11, Fig. 3) in the set 9 was not detected.

The correlation of mass as function of withering to the signal amplitude of the radar sensor results are shown in Fig. 9. This plot displays the significant correlation between the mass of a leaf and its impact on the amplitude response of the PCR. Thus, the linear regression model explains between 95% and 98% variance of the RWC_{sa} in perceived withering condition of a leaf. Fig. 10.

As an additional point of discussion, the results presented in Figs. 5 and 9 demonstrate that the standard error of measurements taken on various sets of plant leaves: Common Ivy, Oakleaf hydrangea, Paniced hydrangea, and English oak less or about 10% for both the gravimetric and the proposed approaches. This means that the measured values of leaf mass and the values obtained using the radar sensor are comparable for both sensing approaches. Thus, the prototype of the sensor based on 60 GHz PCR can be effectively used to determine the relative water

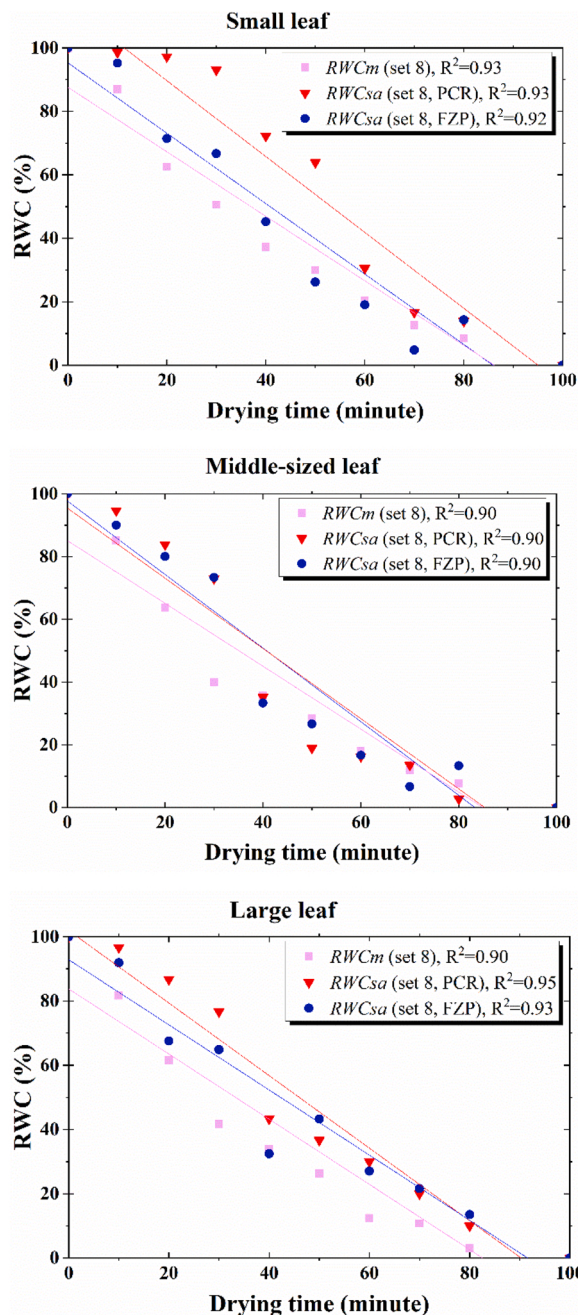


Fig. 7. Plots of water content in three leaves of Oakleaf hydrangea (set 8): small, middle-sized, and a large leaf. Measurements for the gravimetric method $RWCm$ are shown in pink squares; measurements for the radar without a radome $RWCsa$ (PCR) are shown in red triangles; measurements for the radar equipped with the FZP lens $RWCsa$ (FZP) are shown in blue circles.

content (RWC) in leaves, and can estimate the stage of withering without the need to evaluate each individual leaf, but using estimated properties of a fully turgid and after a completely dry representative leaf are taken prior.

This is especially relevant in circumstances where the withering stage of plant leaves may need to be determined for a large amount of species.

Though following facts of data and measurements analysis should be noted and accounted.

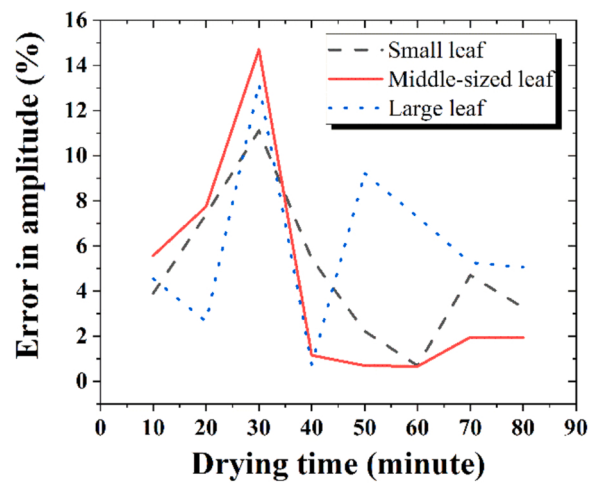


Fig. 8. Plots of the error in amplitude as a function of the time is shown for a single leaf of different sizes of Oakleaf hydrangea (set 8, the leaf which was oven - dried): the dashed - line indicates values for the small leaf, the solid line indicated values for the middle-sized leaf, and the dotted-line indicates values for the large leaf.

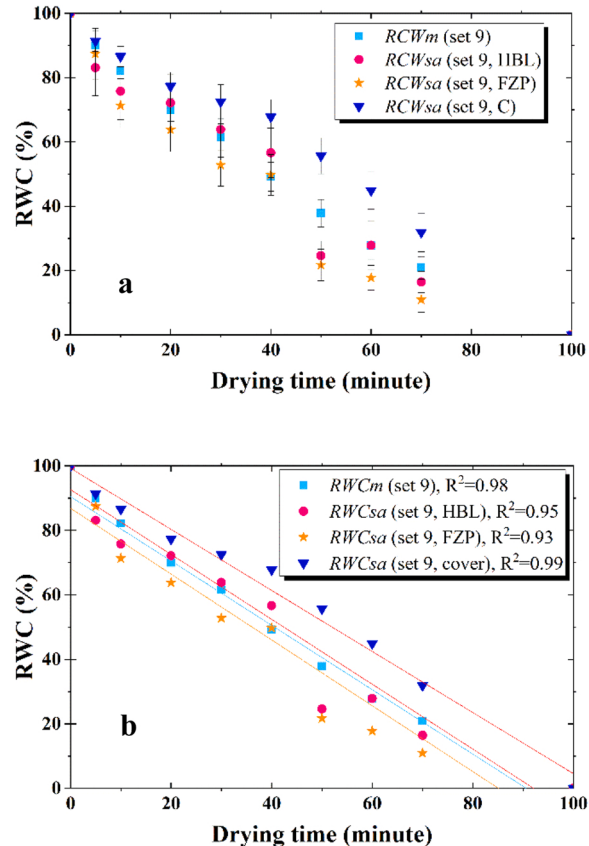


Fig. 9. Plots of water content in English Oak leaves that were oven dried (set 9) as determined using the $RWCsa$ approach using a different radomes: HBL lens (in red circles); FZP lens (in orange stars); a flat cover (in blue triangles) and the gravimetric method $RWCm$ (in light blue squares), as a function of drying time in a sample (the upper figure, a). The R-Squared value to the linear fit is shown inset for each radome and for the absence of one (the upper figure, b).

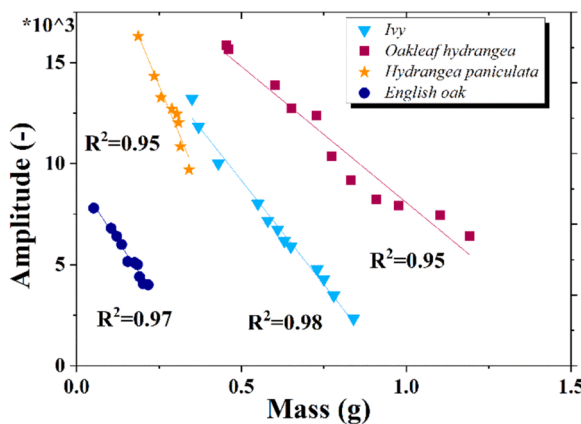


Fig. 10. Plots of the mass loss versus the decrease of the signal amplitude for single - leaf measurements using leaves from Common Ivy (set 1), Oakleaf hydrangea (set 4); Panicked hydrangea (set 6), and English oak (set 9). The R-Squared value to the linear fit is shown inset for each set of samples. The set 9 was measured with applying a flat cover and the rest of measurements were conducted using FZP lens.

Firstly, the larger standard error of set 3 (nine leaves), more specifically, of about 10% shown in the Fig. 5. a is explained by its larger variety in size and form of leaf samples as compared with the set 3 (three leaves) in the same figure, but also with the sets 5 (five leaves) and 7 (five leaves) in Fig. 5. b and Fig. 5. c, respectively.

Secondly, as it was mentioned above, the difference between values for RWC_{sa} and RWC_{m} shown in Figs. 5. b, 7 and 8, using leaves from Oakleaf hydrangea plant can be attributed to their more convex shape and diversity of sizes in comparison to other samples. Thus, during the experiments, a leaf did not fit snugly against the dielectric radome of the prototype (Figs. 1 and 2), but the effect of an air gap as well as other ones like a contrast of surface roughness, leaf temperature, ambient temperature are beyond the scope of this investigations for the proposed application, but can be interesting and useful for the future studies taking into account (17). The identical shape of the curves constructed on the basis of the obtained data for both RWC_{sa} and RWC_{m} can be considered as a proof of the proposed statement.

And lastly, during the method evaluation, some randomness was seen in the data. It can be observed, for instance, in Fig. 5: the average value RWC_{sa} on day 9 and similar point in Fig. 6. b on minute 60 are inconsistent with rest of data. One possible reason for this randomness may be due to inexact angling between the PCR when altering the prototype. Another possible reason may be the angling of the target to the radar beam. The visual detection seems to depend on where the leaf was located in relation to the center of the beam.

Nonetheless, these findings justify further research and development advanced applications and protocols for monitoring the withering condition of leaves using a 60 GHz PCR.

4. Conclusions

The novel sensor application for integrated microwave solutions, has been introduced and evaluated for the online, compact, simple, and cost-effective monitoring of withering conditions of plant leaves.

Besides in this study, the new and effective modelling approach that enables to evaluate withering of leaves by assessing the relative water content (RWC) has been presented. This modelling approach was theoretically described and successfully validated by means of experimental measurements using nine different sets of leaves.

The results demonstrate the enormous potential of millimeter-wave

radar systems, 60 GHz PCR, to provide a non-destructive assay of in situ leaf water content.

An additional value of this study is that it was focused on seeking ways to use the commercial-off-the-shelf (COTS) product solutions to compensate for the lack of monitoring sensors in the food, agriculture and horticulture sectors.

Further studies can be extended to include the effects of radar reflectivity related to a leaf and reveal new details about applications based on a pulse coherent radar (PCR).

Funding

This study was funded by 4TU/Centre for Engineering Education, The Netherlands: Plantenna project.

CRediT authorship contribution statement

N.A. Hoog: Conceptualization, Investigation, Methodology, Formal analysis, Visualization, Writing – original draft. T.E. van den Berg: Methodology, Validation, Visualization, Writing – review & editing. H.S. Bindra: Supervision, Writing – review & editing.

Declaration of Competing Interest

The authors declare that they have no known competing financial interests or personal relationships that could have appeared to influence the work reported in this paper.

Acknowledgment

The authors would like to acknowledge Prof. dr. ir. Bram Nauta and his Integrated Circuit Design (ICD) group at the University of Twente, for the fruitful discussions, support, and providing experiment environments.

References

- [1] S. Veena, S. Poornima, J.V. Remya, A survey on smart sensors in precision agriculture, *Int. J. Adv. Eng. Res. Dev.* 5 (4) (2018) 1143–1144.
- [2] <https://www.pthorticulture.com/en/training-center/volumetric-water-content-sensors/>.
- [3] <http://stesalitte.com/twmac.php>.
- [4] <https://agrihouse.com/secure/shop/item.aspx?itemid=170>.
- [5] <https://agrihouse.com/secure/shop/item.aspx?itemid=134>.
- [6] <https://agrihouse.com/secure/shop/item.aspx?itemid=171>.
- [7] <https://www.metergroup.com/environment/products/phytos-31-leaf-wetness-sensor/>.
- [8] <https://www.campbellsci.com/order/lws>.
- [9] M. Pauli, et al., Miniaturized millimeter-wave radar sensor for high-accuracy applications, *IEEE Trans. Microw. Theory Tech.* 65 (5) (2017) 1707–1715, <https://doi.org/10.1109/TMTT.2017.2677910>.
- [10] R. Ciocoveanu, R. Weigel, V. Issakov, A highly-integrated 60 GHz receiver for radar applications in 28 nm bulk CMOS," 2019 ieee international conference on microwaves, Antennas Commun. Electron. Syst. (COMCAS) 1–5 (2019), <https://doi.org/10.1109/COMCAS44984.2019.8958434>.
- [11] <https://www.infineon.com/cms/en/product/promopages/60GHz/>
- [12] M. Furqan, F. Ahmed, R. Feger, K. Aufinger, A. Stelzer, A 120-GHz wideband FMCW radar demonstrator based on a fully-integrated SiGe transceiver with antenna-in-package, 2016 IEEE MTT-S Int. Conf. Microw. Intell. Mobil. (ICMIM) 1–4 (2016), <https://doi.org/10.1109/ICMIM.2016.7533921>.
- [13] Xanthoula Eirini Pantazi; Dimitrios Moshou; Dionysis Bochtis, Intelligent Data Mining and Fusion Systems in Agriculture - 1st Edition. Print Book & E-Book. ISBN 9780128143919, 9780128143926.
- [14] Jizhan Liu Irfan Abbas, Rana Shahzad Noor Muhammad Faheem, Kashif Ali Solangi Sher Ali Shaikh, Syed Mudassir Raza, Different sensor based intelligent spraying systems in agriculture, *Sens. Actuators A: Phys.* 316 (2020), <https://doi.org/10.1016/j.sna.2020.112265>.
- [15] Luvisi, Electronic identification technology for agriculture, plant, and food. A review, *Agron. Sustain. Dev.* 36 (2016) 13, <https://doi.org/10.1007/s13593-016-0352-3>.

- [16] <https://sensorsandtransmitters.com/sensors/agricultural-horticultural-sensors/>.
- [17] S. Khan and M.M. Hussain, "IoT enabled Plant Sensing Systems for Small and Large Scale Automated Horticultural Monitoring," 2019 IEEE 5th World Forum on Internet of Things (WF-IoT), Limerick, Ireland, 2019, pp. 303–308, doi: 10.1109/WF-IoT.2019.8767309.
- [18] P.B. Elorza, E. Hernando, Francisco Javier Arranz Saiz, B.D. Iglesias, L.R. García, M. Villaruel, J. Villalba and J. García-Hierro., 2011. "Smart Sensing Applications in the Agriculture and Food Industry." 2011.
- [19] Liu Jiangang Yang Guijun, Li. Zhenhong Zhao Chunjiang, Yu. Haiyang Huang Yanbo, Yang Xiaodong Xu Bo, Zhang Xiaoyan Zhu Dongmei, Feng Haikuan Zhang Ruyang, Li. Zhenhai Zhao Xiaoqing, Yang Hao Li Heli, Unmanned aerial vehicle remote sensing for field-based crop phenotyping: current status and perspectives, *Front. Plant Sci.* 8 (1111) (2017), <https://doi.org/10.3389/fpls.2017.01111>.
- [20] M.A. RichardsJ.A. ScheerW.A. Holm(ed.);, 2010. 'Principles of Modern Radar: Basic principles' (Radar, Sonar & Navigation, 2010).
- [21] Sharma, A. Partha, D., 2018. Scientific and Technological Aspects of Tea Drying and Withering: A Review, available at: <https://cigrjournal.org/index.php/Ejournal/article/view/5048> (last ac-cess: 17 August 2020), 2018.
- [22] G. Thamkaew, Ingegerd Sjöholm, Federico Gómez Galindo, A review of drying methods for improving the quality of dried herbs, *Crit. Rev. Food Sci. Nutr.* 61 (11) (2021) 1763–1786, <https://doi.org/10.1080/10408398.2020.1765309>.
- [23] Merrill Ivan Skolnik, Introduction to radar systems. Includes bibliographical references and index. 1. Radar. I. Title. II. Series. TK6575.s477 1980 621.3848 79–15354 ISBN 0-07-057909-1.
- [24] A. Lazaro, M. Lazaro, R. Villarino, D. Girbau, Seat-occupancy detection system and breathing rate monitoring based on a low-cost mm-wave radar at 60 GHz, *IEEE Access* 9 (115403–115414) (2021).
- [25] <https://www.fcc.gov>.
- [26] <https://www.etsi.org>.
- [27] <https://www.powersystemsdesign.com/articles/exploring-advancements-in-industrial-markets-w-60-ghz-radar/22/17649>.
- [28] L. Carneiro de Souza, C.H. de Souza Lopes, R. de Cassia Carlleti dos Santos, A. Cerqueira Sodré Junior, L.L. Mendes, A study on propagation models for 60 GHz signals in indoor environments, *Front. Comms. Net.* 2 (2022), 757842, <https://doi.org/10.3389/frcmn.2021.757842>.
- [29] M. Marcus, B. Pattan, Millimeter wave propagation: spectrum management implications, *IEEE Microw. Mag.* 6 (2) (2005) 54–62, <https://doi.org/10.1109/MMW.2005.1491267>.
- [30] https://www.ti.com/sensors/mmwave-radar/industrial/applications/applications.html?utm_source=google&utm_medium=cpc&utm_campaign=epd-rap-null-portalpagedynamic-cpc-pf-google-wwe&utm_content=portalpagedynamic&ds_k=DYNAMIC+SEARCH+ADS&DCM=yes&gclid=CjwKCAjwmK6IBhBqEiwAocMc8rJQnoim83KxVptJOGXS_3UH_eeSuIZzn9tJNHsLOAv-NtMg4irBoC5M8QAvD_BwE&gclsrc=aw.ds
- [31] <https://www.infineon.com/cms/en/product/promopages/60GHz>.
- [32] https://acconeerpthon-exploration.readthedocs.io/en/latest/sensor_introduction.html.
- [33] V. Issakov, *Microwave Circuits for 24 GHz Automotive Radar in Silicon-based Technologies*, ISBN 978-3-642-13598-9, Springer-Verlag Berlin Heidelberg, 2010.
- [34] Manoj Sharma, Anil Kumar Gautam, Niraj Agrawal, Neeta Singh, Design of MIMO planar antenna at 24 GHz band for radar, communication and sensors applications, ISSN 1434-8411, *AEU - Int. J. Electron. Commun.* 136 (2021), 153747, <https://doi.org/10.1016/j.aeue.2021.153747>.
- [35] Guanghao Sun Keisuke Edanami, Medical radar signal dataset for non-contact respiration and heart rate measurement, ISSN 2352-3409, *Data Brief.* 40 (2022), 107724, <https://doi.org/10.1016/j.dib.2021.107724>.
- [36] A. Tzadok, A. Valdes-Garcia, P. Pepejugoski, J.-O. Plouchart, M. Yeck, H. Liu, AI-driven Event Recognition with a Real-Time 3D 60-GHz Radar System, 2020 IEEE/MTT-S Int. Microw. Symp. (IMS) (2020) 795–798, <https://doi.org/10.1109/IMS30576.2020.9224112>.
- [37] <https://www.nxp.com/applications/automotive/adas-and-highly-automated-driving/automotive-radar-systems:RADAR-SYSTEMS>, <https://www.microwavejournal.com/articles/33705-comprehensive-survey-of-77-79-ghz-automotive-radar-companies-sensors-and-ics>, http://www.imst/en/news/Radar_new2016.php,
- [38] R. Gourova, O. Krasnov, A. Yarovoy, Analysis of rain clutter detections in commercial 77 GHz automotive radar, 2017 Eur. Radar Conf. (EURAD) (2017) 25–28, <https://doi.org/10.23919/EURAD.2017.8249138>.
- [39] C. Shao, F. Cheng, S. Mao, J. Hu, Vehicle intelligent classification based on big multimodal data analysis and sparrow search optimization, *Big Data* (2022) doi: 10.1089/big.2021.0311. Epub ahead of print. PMID: 35510929.;
- [40] N. Bahmani, M. Rouvala, A. Kaarna, Vital sign detection using short-range mm-wave pulsed radar, 2021 IEEE 3rd Glob. Conf. Life Sci. Technol. (LifeTech) (2021) 512–516, <https://doi.org/10.1109/LifeTech52111.2021.9391910>.
- [41] Z. Zhang, X. He, J. Huang and H. Yuan, Parking detection using combined magnetic sensor and pulsed coherent radar, *IEEE Internet Things J.*, doi: 10.1109/JIOT.2022.3151987.
- [42] L.O. Phager, S. Heunisch, H. Dahlberg, A. Evertsson, L. Wernersson, Pulsed millimeter wave radar for hand gesture sensing and classification, Art no. 3502404,
- [43] IEEE Sens. Lett. 3 (12) (. 2019) 1–4, <https://doi.org/10.1109/LESENS.2019.2953022>.
- [44] M. Smithson, M.P.-L. Ooi, L. Gris, Y.C. Kuang, M. Manley-Harris, S.H. Lim, Investigating the use of low-cost and Low-power millimeter wave RADAR to improve quality of tomato harvesting, 2021 IEEE Int. Instrum. Meas. Technol. Conf. (I2MTC) (2021) 1–6, <https://doi.org/10.1109/I2MTC50364.2021.9459975>.
- [45] <https://www.4tu.nl/plantenna/>
- [46] R.E. Smart, Rapid estimates of relative water content, *Plant Physiol.* 53 (2) (1974), 258–60. doi: 10.1104/pp.53.2.258. PMID: 16658686; PMCID: PMC541374.
- [47] H.D. Barrs, P.E. Weatherley, A Re-Examination of the relative turgidity technique for estimating water deficits in leaves, *Aust. J. Biol. Sci.* 15 (1962) 413–428, <https://doi.org/10.1071/B19620413>.
- [48] F.T. Ulaby and R.P. Jedlicka, Microwave Dielectric Properties of Plant Materials, *IEEE Transactions on Geoscience and Remote Sensing*, vol. GE-22, no. 4, pp. 406–415, July 1984, doi: 10.1109/TGRS.1984.350644.
- [49] J.H. Lambert, *Photometria sive de mensura et gradibus luminis, colorum et umbrarum*, Eberhardt Klett (1760).
- [50] A. Beer, Bestimmung der Absorption des rothen Lichts in farbigen Flüssigkeiten, *Ann. der Phys. und Chem.* 86 (1852) 78, <https://doi.org/10.1002/andp.18521620505>.
- [51] L.C. Santos, F.N. dos Santos, R. Morais, C. Duarte, Potential non-invasive technique for accessing plant water contents using a radar system, *Agronomy* 11 (2021) 279, <https://doi.org/10.3390/agronomy11020279>.
- [52] <https://www.acconeerp.com>
- [53] https://www.codicco.com/media/productattach/g/e/getting_started_guide_lenses_484978_5.pdf
- [54] <https://docs.acconeerp.com/en/latest/services/index.html>
- [55] <https://developer.acconeerp.com/download/hardware-and-physical-integration-guideline-pdf>
- [56] <https://www.homegeek.com/p-h18732.html>
- [57] <https://acconeerpthon-exploration.readthedocs.io/en/latest/services/envelope.html#envelope-service>
- [58] <https://developer.acconeerp.com/developer/documents-learning/lh112/>
- [59] T. Van Emmerik, S.C. Steele-Dunne, J. Judge, N. Van De Giesen, Dielectric response of corn leaves to water stress, *IEEE Geosci. Remote Sens. Lett.* 14 (1) (. 2017) 8–12, <https://doi.org/10.1109/LGRS.2016.2606662>.
- [60] L. González, M. González-Vilar, Determination of relative water content, in: M. J. Reigosa Roger (Ed.), *Handbook of Plant Ecophysiology Techniques*, Springer, Dordrecht, 2001, https://doi.org/10.1007/0-306-48057-3_14.
- [61] <https://patents.google.com/patent/US8986770B2>: Process for fabricating leaf tea products.
- [62] I. Oshima, J. Spigulis, Beer-Lambert law for optical tissue diagnostics: current state of the art and the main limitations, *J. Biomed. Opt.* 26 (10) (2021), 100901, <https://doi.org/10.1117/1.JBO.26.10.100901>.
- [63] J.D. Taylor, *Introduction to Ultra-Wideband Radar Systems*; Edition 1st Edition; First Published 1995; eBook Published 24 September 2020; Pub. Location Boca Raton.
- [64] G. Scarchilli, E. Gorgucci and V. Chandrasekar, Detection and estimation of reflectivity gradients in the radar resolution volume using multiparameter radar measurements, in *IEEE Transactions on Geoscience and Remote Sensing*, vol. 37, no. 2, pp. 1122–1127, March 1999, doi: 10.1109/36.752230.
- [65] Randy G. Victor Maddox, John D. Westbrooks, English Ivy Byrd, (*Hedera helix L.*), Tech. Rep. (2018), <https://doi.org/10.13140/RG.2.2.20982.24649>.
- [66] A. Sherwood, M.D. Clark, S.C. Hokanson, S.C. Oakleaf hydrangea (*Hydrangea quercifolia Bartr.*): horticulture, *Genet. Breed., Conserv. Hortic. Rev.* 49 (49) (2021) 1.
- [67] N. Lancaster, W. Wesley, *Hydrangea paniculata*, *RHS Plant Trials Bull.* 2 (2–15) (2008).
- [68] L. Meyer, C. Brischke, E. Melcher, K. Brandt, M.-T. Lenz, A. Soetbeer, Durability of English oak (*Quercus robur L.*) – comparison of decay progress and resistance under various laboratory and field conditions, *Int. Biotdegrad. Biodegrad. (Part B)* (2014) 79–85. ISSN 0964-8305, <https://doi.org/10.1016/j.ibiod.2013.06.025>.

Natalia A. Hoog (Antonyuk) studied and received her Engineer Diploma within specialization "Organization and Technology of Information Security", at Tomsk State University of Control Systems and Radioelectronics (TSUCSR), Russia in 2002. In 2002 – 2006 she was a member of international project The Netherlands (TU Delft)-Russian (TSUCSR) with research activities in the area of advanced Ground-Penetrating Radar (GPR) technology. In 2014 she received Ph.D. degree from the University of Twente, the Laboratory of Biosensors, the Lab-on-a-Chip group, Enschede, The Netherlands. From 2015–2020 she worked for Omnidarad B.V./Staal Technologies B.V. at different positions, as a Technical project manager and as Director Radar Technology in Eindhoven, the Netherlands. Since September 2020, she is a Postdoctoral researcher at the Integrated Circuit Design group of the University of Twente. Her expertise lies in microwave sensing engineering, semiconductor packaging, radar, antenna – based sensors and she has (co-) authored scholarly articles, conference papers, and 7 patents. In 2013 her research work at Wetsus - European center of excellence for sustainable water technology was awarded the Marcel Mulder prize.

Tomas van den Berg studied Chemistry within specialization Biochemistry, at Rijksuniversiteit Groningen, then specialized as Msc. in Molecular Biology and Biotechnology, graduating in 2012. From 2012 he started his Ph.D. in Biophysics of Photosynthesis in the group of Prof. Roberta Croce at the Vrije Universiteit Amsterdam. From 2016 he started to consult companies, mainly in the festival industry, on the methods to reduce the carbon footprint of their catering via his start-up Foodprints. Since 2019 he is a Postdoctoral researcher at the Integrated Devices and Systems group of the University of Twente within the Plantenna consortium working on plant based sensors. His expertise lies in photosynthesis research, Chlorophyll fluorescence microscopy and spectroscopy and stomatal functioning.

Harijot Singh Bindra (S'16) received the B.Tech. degree in electronics and communication engineering from Punjabi University, Patiala, India, in 2008, and the M.Tech. degree

in VLSI design from the IIT, Delhi, India, in 2012. In 2019 he obtained his PhD degree cum laude from University of Twente, Enschede, The Netherlands where he is currently an Assistant Professor at the Integrated Circuit Design group. From 2008–2010, he was a Scientist with the Indian Space Research Organization, Chandigarh, India, where he was involved in the semi-conductor design and fabrication facility. He was a Senior Design Engineer at Cadence Design Systems, Noida, India, from 2012 to 2014, where he worked on high-speed serial links, clock and data recovery circuits and equalizers. His current research interests include ADCs, low-voltage low-energy circuit design, equalizers, and clocking and data recovery circuits. He is a recipient of the University Gold Medal in B. Tech. degree and was awarded the graduate scholarship during his Master's degree from Cadence Design Systems Inc. He serves as a reviewer for the IEEE Journal of Solid-State Circuits and is currently an Associate Editor for Transactions on Circuits and Systems - I